Eur. Phys. J. D (2014) 68: 308
DOI: 10.1140/epjd/e2014-50257-5

THE EUROPEAN PHYSICAL JOURNAL D

Regular Article

Spectral investigations on the influence of silver nanoparticles on the fluorescence quenching of 1,4-dimethoxy-2,3-dibromomethylanthracene-9,10-dione

Singlepatti Ramasamy Kavitha[1], Mahalingam Umadevi[1,a], Patrice Vanelle[2,3], Thierry Terme[2,3], and Omar Khoumeri[2,3]

[1] Department of Physics, Mother Teresa Women's University, 624101 Kodaikanal, Tamil Nadu, India
[2] Laboratoire de Pharmaco-Chimie Radicalaire, Faculté de Pharmacie, Aix-Marseille University, CNRS,
[3] Institut de Chimie Radicalaire ICR, UMR 7273, 27 Boulevard Jean Moulin, 13385 Marseille Cedex 05, France

Received 30 March 2014 / Received in final form 29 July 2014
Published online 21 October 2014 –

Abstract. Silver nanoparticles (Ag NPs) of different sizes from 9 to 17 nm were synthesized by Creighton method and characterized using UV-vis spectroscopy and high resolution transmission electron microscopy (HRTEM). Fluorescence quenching of 1,4-dimethoxy-2,3-dibromomethylanthracene-9,10-dione (DMDBMAD) in methanol has been studied by fluorescence spectroscopy combined with UV-vis absorption spectroscopic techniques. It has been observed that the fluorescence intensity of DMDBMAD decrease with increase in the size of the Ag NPs. The quenching rate constant and association constant were determined using Stern-Volmer and Benesi-Hildebrand plots. The Stern-Volmer plot suggested that the quenching of DMDBMAD fluorescence by silver NPs was a dynamic process. The obtained value of the association constant infers that there is an association between DMDBMAD and the Ag NPs. Using Förster resonance energy transfer (FRET) theory, the distance between the donor (DMDBMAD) to acceptor (Ag NPs) and the critical energy transfer distance were obtained. Long range dipole-dipole interaction between the excited donor and ground state acceptor molecules is the dominant mechanism responsible for the energy transfer.

1 Introduction

Anthraquinone is the most important quinone derivative of anthracene. It is a group of aromatic compound containing two opposite carbonyl groups (C = O) and the other two pairs of carbon atoms linked by Vinylene group (–CH = CH) in a six membered unsaturated ring. Quinones are one of such compounds which occur naturally in some plants (aloe latex, senna and rhubarb), fungi, lichens, and insects, where they serve as a basic skeleton for their pigments. Quinones and their derivatives comprise an important class of redox mediators and electron-transfer quenchers. Anthraquinones are naturally colored and therefore have been extensively used as an antioxidant in medicine, a catalyst in paper industry and a coloring material in textile industry. They are considered together with other traditional colorants for application in technologies such as optical data transmission storage and solar energy conversion [1]. These derivatives are of major importance in obtaining luminescent materials with potential applications as materials for lasers, paints, luminescent photolayers and light-emitting devices [2]. They are also used as fluorescent probes in order to investigate protein-ligand interactions by fluorescence spectroscopic techniques [3]. These molecules have important applications as a prominent family of pharmaceutically active and biologically relevant chromophores, as an analytical tool for the determination of metals, and in many aspects of electrochemistry. The quinone structural fragment is often found in naturally occurring compounds which exhibit antitumour, antibacterial, malaricidal and fungicidal actions. These are important class of a quinone system that absorbs light in the visible region [4].

Investigations of metal NPs have attracted significant attention because of their unusual size dependent optical and electronic properties. Presently there is intense interest in the optical properties of Au and Ag colloids. These colloids display bright colors due to the surface Plasmon resonance (SPR) absorption, which is in fact due to a combination of absorption and scatter [5]. The color of the NP is found to depend on the shape and size of the nanoparticle and dielectric constant of the surrounding medium, leading to many studies on their synthesis and applications. The color of the metal NPs are mainly due to the collective oscillation of the electrons in the conduction band, known as the surface plasmon oscillation. The oscillation frequency is usually in the visible region for Au and Ag giving rise to the strong SPR absorption.

[a] e-mail: ums10@yahoo.com

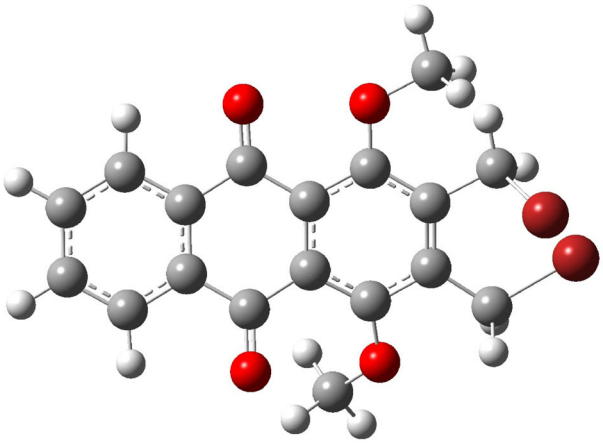

Fig. 1. Structure of 1,4-dimethoxy-2,3-dibromomethylanthracene-9,10-dione (DMDBMAD).

These optical properties make metallic colloids potentially useful in sensing and imaging techniques [6].

The interactions of fluorophores with metal nanoparticles results in the fluorescence enhancement/quenching, increased photostability, decreased lifetime because of increased rates of system radiative decay and increased transfer distances for FRET [7]. The enhancement or quenching of the fluorescence emission of molecules near a metal surface arises from interactions with surface plasmon resonance in the metal particles. These interactions may also result in shortening of the excited-state lifetime thus improving the photostability of the dye. The optical properties of a fluorescent molecule located near the metal nanoparticles are affected by the near-field electro dynamical environment [8]. This can cause an enhancement or quenching of the fluorescence depending on the distance between the molecule and the metal surface. In the case of fluorescent molecules located at very short distances from a metal surface, non-radiative energy transfer to surface plasmon in the metal takes place [3]. The quenching of fluorescence provides useful information on the nature of interaction between the fluorophore and the quencher. Our group has studied the spectroscopic characteristics of anthraquinone derivatives in Ag NPs environment [9–14]. The dye doped Ag NPs have captured recent interest in medical diagnostic, proteins, membranes, sensing, labeling, optical data transmission storage, bioanalytical probes, solar energy conversion and dye synthesized solar cells. The biological applications of dye doped quenchers and fluorescence quenching property motivated the group to conduct the study. In the present case, we got interested in the effect of silver nanoparticles on the fluorescence properties of DMDBMAD (Fig. 1).

2 Experimental

2.1 Materials

Silver nitrate ($AgNO_3$, 99.5%), sodium borohydride ($NaBH_4$, 95%) and Rhodamine 6G were purchased from MERCK. Spectral grade methanol (CH_3OH) was purchased from NICE. All the chemicals were of Analytical Grade and used as purchased without further purification. Doubly distilled water was used throughout the experiment. All glasswares were properly washed with distilled water and dried in hot air oven before use.

2.2 Preparation of Ag NPs

Silver colloidal sol was prepared by Creighton method [15] at different $AgNO_3$ concentration ratios. In brief, $AgNO_3$ solution and $NaBH_4$ solution were individually prepared by dissolving 0.0545 mM of $AgNO_3$ in 50 ml of distilled water and 3 mM of $NaBH_4$ in 100 ml of distilled water with vigorous stirring (1 h). Both the solutions are kept separately in ice cooled temperature (–1 °C). 50 ml of $AgNO_3$ solution was added dropwise to 100 ml of $NaBH_4$ solution and the mixture was shaken vigorously until glassy yellow solution was obtained (S1). It was repeated for different concentration of silver nitrate solution (0.1, 0.1384 and 0.1714 mM) (S2, S3 and S4) at constant concentration of $NaBH_4$ solution (3 mM). The silver colloid was stored in a dark place (20 °C).

2.3 Synthesis of DMDBMAD

1,4-dimethoxy-2,3-dibromomethyl anthracene-9,10-dione were prepared according to the literature [16]. In brief, to a solution of 1,4-dimethoxy-2-methylanthracene-9,10-dione (1 g, 3.52 mmol) in carbon tetrachloride (100 mL) was added N-bromosuccinimide (1.89 g, 10.62 mmol) and catalytic amount of benzoyl peroxide. The reaction mixture was heated to 80 °C and irradiated with a 300 W sun lamp for 7 h. After cooling and evaporation, the residue was dissolved in chloroform and washed with water. The organic layer was dried over magnesium sulfate and the solvent was removed under vacuum. Purification on silica gel eluting with ethyl acetate/petroleum ether (1/2) gave 1.34 g (87%) of DMDBMAD as yellow solid. This synthetic method was based on the following chemical reaction,

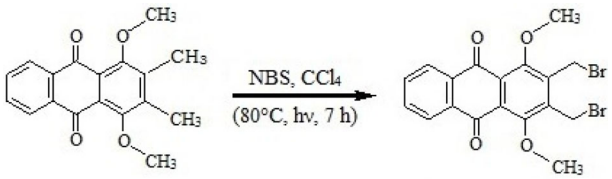

(DMDBMAD)

The concentration of DMDBMAD in methanol was maintained at 0.02 mM throughout the experiment. To investigate the influence of Ag NPs on DMDBMAD, the dye and quencher solution have been taken in 1:1 volume ratio.

2.4 Methods of characterization

Optical absorption spectra were recorded using a Shimadzu UV-1700 pharmaspec UV-vis spectrophotometer. Jobin Yvon Flurolog-3-11 Spectrofluorometer was

Table 1. Photo-physical properties of Ag NPs and Energy transfer parameters of DMDBMAD in Ag NPs.

S.No	Concentration of $AgNO_3$ (mM)	SPR peak of Ag NPs (nm)	FWHM (nm)	Fluorescence quantum yield (φ)	J (λ) (cm^3 L mol^{-1})	R_0 (nm)	r_0 (nm)	E (%)
1.	0.0545 (S1)	393	40	0.0059	2.11×10^{-14}	198	104	100
2.	0.1 (S2)	396	56	0.0022	1.72×10^{-14}	191	97	96
3.	0.1384(S3)	399	64	0.0013	1.37×10^{-14}	184	90	95
4.	0.1714 (S4)	401	66	0.0005	1.25×10^{-14}	181	87	92

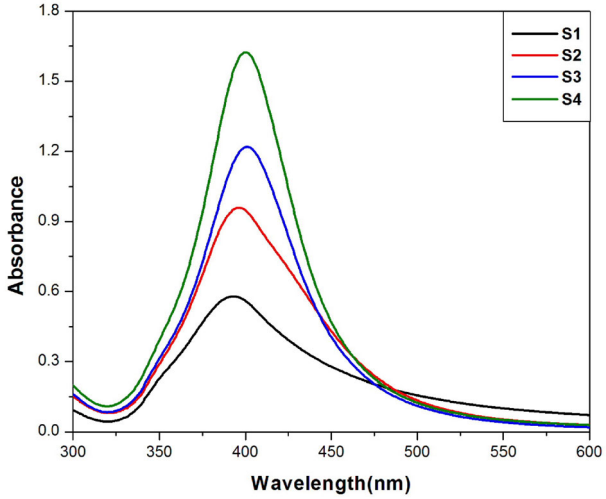

Fig. 2. Optical absorption spectra of Ag NPs.

used to record the emission spectra. The excitation wavelength of DMDBMAD is 330 nm. The morphology and the size of the nanoparticles were determined using a JEOL JEM 2100 high resolution transmission electron microscope operating at 200 kV. All the measurements were performed at room temperature.

2.5 Fluorescence quantum yield

The relative fluorescence quantum yield (φ_{rel}) [3] of the sample in terms of reference sample (φ_0) is

$$(\varphi_{rel}) = \left(\frac{F}{F_0}\right)\left(\frac{OD_0}{OD}\right)\left(\frac{n}{n_0}\right)\varphi_0$$

where F and F_0 are the integrated fluorescence intensities, OD and OD_0 are the optical densities and n and n_0 are the refractive indexes for Rhodamine 6G in methanol. The relative fluorescence quantum yield (φ_{rel}) in which Rhodamine 6G was used as fluorescence standard ($\varphi = 0.94$). In the present case, the fluorescence quantum yield of DMDBMAD in methanol was found to be 0.0154.

3 Results and discussion

3.1 Optical absorption spectral studies: Ag NPs

UV-vis absorption spectra of prepared Ag NPs at different concentrations are shown in Figure 2. Table 1 shows the observed surface plasmon resonance (SPR) peak and full width at half maximum (FWHM) values of the prepared Ag NPs. The maximum absorption peak appears around 400 nm, which is due to the characteristic surface plasmon resonance of Ag NPs [17]. Conduction electrons on the surface of silver NPs undergo a collective oscillation known as SPR due to its strong interaction with the incident light. For spherical NPs much smaller than the wavelength of light, the electromagnetic field is uniform across the particle causing all the conduction electrons to move in-phase producing only dipole-type oscillations manifested by a single, narrow peak in the SPR spectrum. As the size increases and deviates from the spherical shape, the field across the particle becomes non-uniform. Phase retardation then broadens the dipole resonance and excites higher multi-pole resonances. Further, the oscillating electrons induce polarisation of the opposite direction in the surrounding medium which reduces the restoring force for the electrons resulting in a shift in the SPR [18].

An absorption peak at around 400 nm observed generally is attributed to the SPR excitation of Ag NPs. Mie [19] and Wang et al. [20] have carried out theoretical studies on the dependence of UV absorption maximum on the size of metal NPs. The spectrum can exhibit a shift towards the red end or the blue wavelength depending upon the particle size, shape, state of aggregation and the surrounding dielectric medium [21]. Absorption spectra obtained for the sample S4 indicates that the size of the particles must be large than that of S1. This result is in consistent with the TEM images of the colloidal silver. As the concentration of silver nitrate increases, the surface plasmon band shifts towards the red (longer) wavelength and its FWHM increases. The plasmon peak and full width at half maxima depends on the extent of colloid aggregation [22]. In the present case, the size of prepared silver nanoparticles increases as the concentration of silver nitrate increases. The observed plasmon band observed around 400 nm suggests that the Ag NPs are spherical in shape [23]. For a small particle, the maximum absorbance intensity and bandwidth of the SPR peak rely on the surroundings of the medium. When the Ag NPs strongly dominate the matrices condition, a large broadening of the SPR occurs. This would result in blue shift characteristics. Similarly, a red shift with small broadening would take place when low interactions occur between the Ag NPs and matrices. This would result in red shift characteristics [24].

Henglein [25] reported the substantial decrease in red shift of Ag NPs SPR band, while studying the effect of

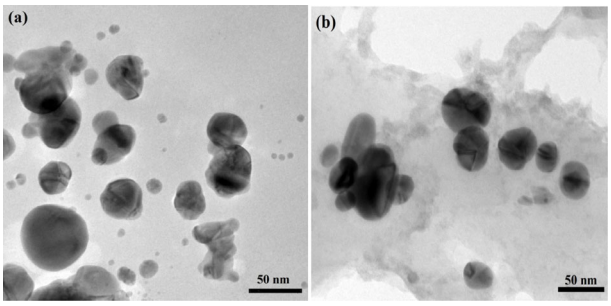

Fig. 3. TEM micrographs of the silver nanoparticles. (a) S1 (the scale bar corresponds to 50 nm) and (b) S4 (the scale bar corresponds to 50 nm).

excess Ag^+ ion on Ag NPs. It has been explained in terms of decrease of electron density on the nanoparticles surface upon chemisorption of silver ions. Since the wavelength of the absorption maximum is inversely proportional to the density of free electrons in the metal for particles of a few nanometers, it is independent of size. In the present case, as the concentration of $AgNO_3$ increases density of free electrons in the silver decreases which are chemisorbed on the surface of nanoparticle and thus the plasmon responsible for SPR shift.

3.2 Morphological analysis of Ag NPs

Transmission electron micrographs in Figures 3a and 3b display the silver nanoparticles obtained under different concentrations S1 and S4, respectively. The average size of these nanoparticles is approximately ranged from 9 nm (S1) to 17 nm (S4) and this result was also confirmed by UV-vis spectra of Ag NPs. The average size increased with elevated concentration which was consistent to the red shift (longer wavelength) of the absorption peaks in the UV-vis spectra. The degree of size dispersity of silver NPs increased with increasing Ag concentration (Tab. 1). The formation of large particles with higher size dispersity could be attributed to the silver migration and aggregation. The migration and aggregation of the Ag particles might be driven by the instability of silver atoms due to their high surface free energy. Their aggregation would produce thermodynamically stable clusters [26,27]. The prepared silver NPs shows twinning in the crystalline structure. Twinning is one of the most commonly noticed planar defects in nanocrystals, and is frequently observed for metallic nanocrystals of face centered cubic (fcc) structure. It occurs when two subgrains share a common crystallographic plane. The structure of one subgrain is then a mirror image of the other through the twinning plane. The silver nanoparticles were found to be more or less spherical, elongated in shape and the nanoparticles are poly-dispersed. It was also observed that the majority of the particles in this case exhibit internal structure, characterized by strain effects and stacking faults (multiple-twinned nanoparticles) with five-fold symmetry, i.e. decahedral and icosahedral particles. Because of this five-fold axis, strain was induced in the particle to fill the gap.

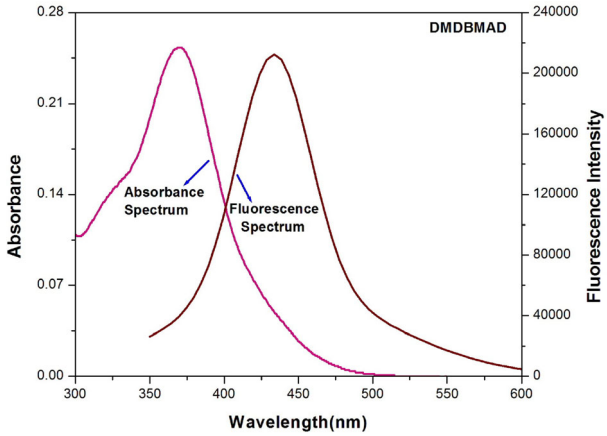

Fig. 4. Optical absorption and fluorescence emission spectra of DMDBMAD in methanol.

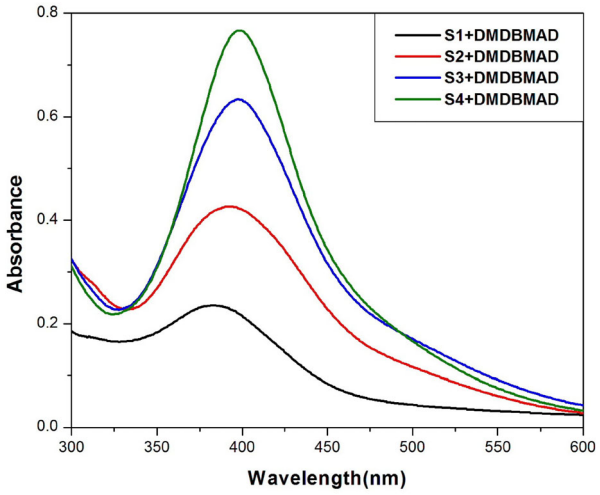

Fig. 5. Optical absorption spectra of DMDBMAD in Ag NPs.

When the particles are smaller in size, the multiple twinning is the favorable structural configuration. It may be due to the smaller surface and volume energies [28].

3.3 Optical absorption spectral studies: DMDBMAD in Ag NPs

Figures 4 and 5 represent the absorption spectrum of DMDBMAD in methanol and absorption spectra of DMDBMAD in different sizes of Ag NPs, respectively. Absorption spectrum of DMDBMAD in the methanol shows a broad band in the visible region from 300 to 400 nm with one strong peak observed at 370 nm. The absorption spectra of DMDBMAD in different sizes of Ag NPs show broad band in the region 300 to 500 nm. When donor molecule is added into silver sol, the original features of the spectra have been changed and the silver plasmon peak is shifted towards the longer wavelengths and its intensity decreases, i.e., damping and broadening of the plasmon band is observed. The major reason for SPR broadening is electron surface scattering which may be enhanced for very

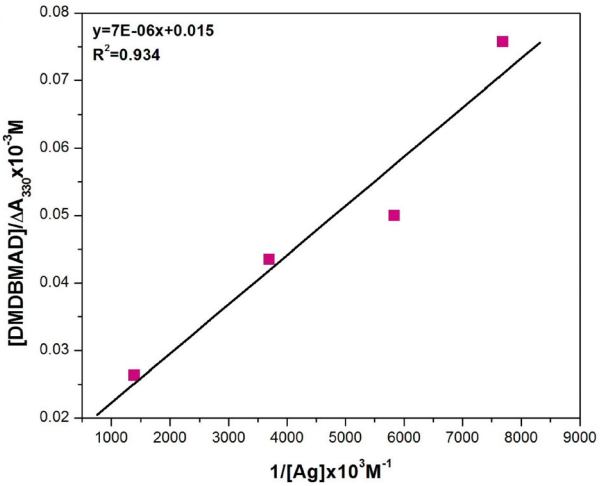

Fig. 6. Benesi-Hildebrand plot.

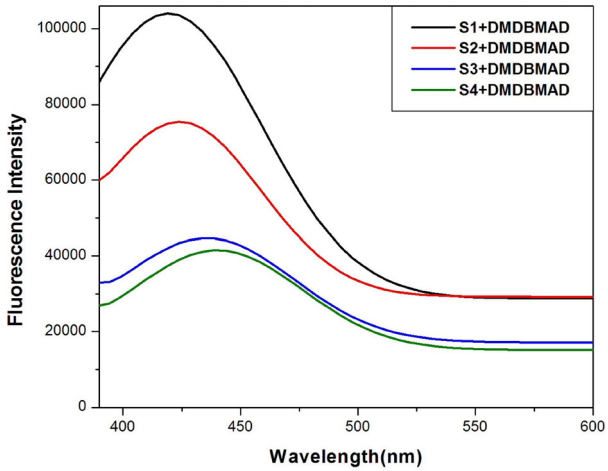

Fig. 7. Fluorescence emission spectra of DMDBMAD in Ag NPs.

small clusters [29]. This change in spectral shift and band broadening of the surface plasmon band reveals that these DMDBMAD may bind on the silver surface. The damping of the silver plasmon band indicates the attachment of the DMDBMAD molecule on the nanoparticles surface. The interaction of silver nanoparticles with DMDBMAD alters the electron density of the Ag NPs, thereby directly affecting the absorption of the surface bound DMDBMAD as well as surface plasmon absorption band.

3.4 Benesi-Hildebrand approach

The interaction between DMDBMAD and Ag NPs was investigated by determining the association constant (K_{ass}). The association constant can be measured by various spectroscopic methods. Among those methods, Benesi-Hildebrand approach [30] was used. Using these spectral shifts the binding constant of DMDBMAD with Ag NPs in the ground state can be calculated. By this approach, the association constant for the complex formed between Ag NPs and DMDBMAD is obtained by analyzing the optical absorption spectral changes. The association constant of $K_{ass} = 2055\ M^{-1}$ was obtained from the plot of [DMDBMAD]/ΔA_{330} vs. 1/[Ag] as shown in Figure 6, where ΔA_{330} is the changes in absorbance of DMDBMAD with and without Ag NPs at 330 nm and [Ag] is the concentration of silver. The value of association constant observed in this experiment suggests that there is an association between DMDBMAD and Ag NPs [9–14].

3.5 Fluorescence spectral studies

The fluorescence emission spectrum of DMDBMAD in methanol and fluorescence spectra of DMDBMAD in different sizes of Ag NPs is shown in Figures 4 and 7, respectively. The observed fluorescence quantum yield of DMDBMAD in different sizes of NPs has been reported in Table 1. Fluorescence emission spectrum of DMDBMAD in methanol shows a broad band in the visible region 350–550 nm with strong peak observed at 433 nm. The fluorescence spectra of DMDBMAD in different sizes of Ag NPs show broad band in the region 390–530 nm. The DMDBMAD molecules added with the nanoparticles are in thermodynamical equilibrium and the only fluorescent component arises from the free DMDBMAD molecules in the solution. And hence the fluorescence is due to the unbound probe molecules in the system. With increase in the concentration of silver nanoparticles, more dye molecules were adsorbed on silver surface and hence the fluorescence of the dye was quenched. This leads to a situation that the existence of less number of free probe dye molecules and so the number of free fluorophores decreases and thus the decrease in fluorescence intensity. In the presence of Ag NPs, the fluorescence intensity of the SPR band and quantum yield of DMDBMAD decreases (Tab. 1) without any new broad band in the fluorescence emission spectra which reveal that the DMDBMAD bound to Ag NPs failed to exhibit intermolecular interaction [9–14]. The lowered intensities show that Ag NPs are responsible for this quenching effect. The smaller Ag NPs of S1 showed greatest quenching, while the larger NPs like S4 quenched to a lesser extent. This quenching in the fluorescence intensity is mainly due to energy transfer from the DMDBMAD to the Ag NPs. When the donor molecules are in close vicinity of the acceptor molecule, resonance energy transfer occurs resulting in reduced fluorescence intensity [31].

Quenching is a process which reduces the lifetime of the excited state. A reduction in the lifetime usually implies a decrease in the quantum yield. Some of the processes which reduce the quantum yield are: dynamic (collisional) quenching, static quenching and energy transfer. Both quenching requires contact between the fluorophore and the quencher. Thus, these methods are useful to measure rates of diffusion and exposure of fluorescent species to the quencher. Static quenching is observed when a fluorophore forms a complex with the quencher. It is normally assumed that complex formation will prevent

the fluorophore from emitting a fluorescent photon, however those fluorophores which are not complexed with the quencher emit normally with the same lifetime as in the absence of the quencher [3].

Fluorescence quenching may also result from a photo induced electron transfer process between the excited DMDBMAD and the Ag NPs. The interaction with the dye and the excited state surface reactions may lead to morphological changes of the Ag NPs. The surface plasmon efficiently acts as energy acceptor even at a distance of 1 nm between the probe molecules and the metal surface. Ag NPs also have a continuum of electronic states and exhibit energy transfer behavior as excited state quenchers. The observed changes in the absorbance of the absorption spectrum and fluorescence intensity reflects the alteration of the electronic properties of the DMDBMAD chromophore as it binds to the Ag NPs which acts as a excited state quencher. The DMDBMAD has a high emission quantum yield in the absence of NPs, the dominant effect for the quenching of excited state of DMDBMAD in Ag NPs may be due to radiative energy transfer to the Ag surface. Geddes et al. [32] described the effect of Ag NPs on near the fluorophores. When the DMDBMAD fluorophore-Ag distance is increased, both fluorescence quenching and enhancement have been observed [33]. Ditlbacher et al. [34] explained the changes of molecular fluorescence near Ag NP. When using DMDBMAD fluorophore as local probes of the surface plasmon field of metallic NPs, in the close proximity of an Ag, the fluorescence rate of the molecules is a function of the distance between the probe molecule and the metal surface. When in direct contact with the metal, the fluorescence of molecules is completely quenched.

The energy transfer and electron-transfer processes are the major deactivation processes for quenching of excited state DMDBMAD fluorophores on the Ag surfaces. Excited state fluorophore behaves as an oscillating dipole. When these fluorophores are in close proximity to the metal Ag NPs, the rate of emission and the spatial distribution of the radiating energy are modified. The electric field felt by the DMDBMAD fluorophores are affected by the interaction of the incident light with the nearby Ag surface. These interactions can increase/decrease in the field felt by the DMDBMAD fluorophore and the increase/decrease in the radiative decay rate [3] will result in many desirable effects such as increased quantum yield and decreased lifetime. When a metal NPs has been excited and is oscillating in the incident electromagnetic field, the excited DMDBMAD fluorophore molecules may have a fluctuating electric dipole moment and causes the radiation [35]. This radiation from dipole moment of excited fluorophore molecule provides the path for radiative decay. On the other hand, the joule heating plasmon absorption caused by these fields provides the path for non-radiative decay channels [36]. The competition between radiative and non-radiative decay energy transfer affects the fluorescence emission of the DMDBMAD fluorophore molecules located near the Ag NPs due to joule heating and surface plasmon absorption.

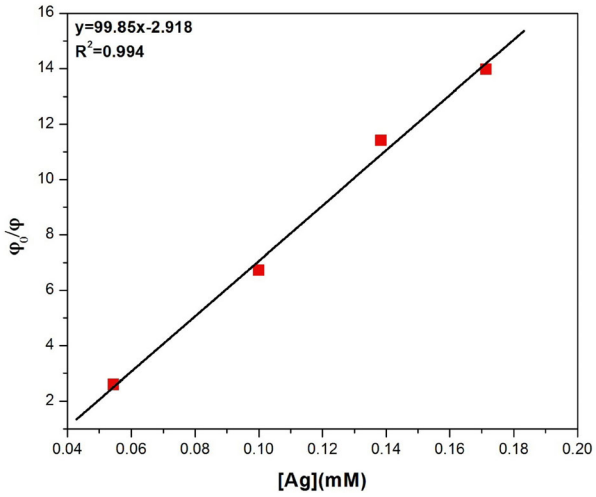

Fig. 8. Stern-Volmer plot.

In the present case, non-radiative decay due to joule heating and surface plasmon absorption takes the dominating effect which in turn decreases the fluorescence emission and fluorescence quantum yield of DMDBMAD. This non-radiative decay can also be theoretically studied using the Förster energy transfer theory [37]. When Ag NPs is added into the DMDBMAD, the DMDBMAD molecules would tend to adsorb on the silver surface due to physisorption. As the size of the particle increases, the surface area decreases which in turn decreases the number of DMDBMAD molecules that would adsorb on the metal surface. The probability of this energy transfer depends on the overlap of the donor molecules with the absorption spectrum of the acceptor molecules. The excitation of the electronic plasma resonance increases the absorption rate. Moreover the molecular emission dipole excites the plasma resonance which increases the rate of radiative decay. In addition, the non-radiative decay provides damping effect when latter process increases, the quenching of fluorescence is observed. The metallic surface induces a strong quenching of molecular fluorescence due to the electromagnetic coupling between the Ag and the fluorophore [38].

3.6 Stern-Volmer approach

The quenching rate constant has been calculated from Stern-Volmer plot. The Stern-Volmer equation accounting for both static and dynamic quenching is generally written as $\varphi_0/\varphi = 1 + K_{SV}$ [Ag] [3] where $K_{SV} = K_S + K_D$ where K_S and K_D are the static and dynamic quenching constants, respectively, φ_0 and φ are the fluorescence quantum yield of DMDBMAD in the absence and presence of quencher [Ag], respectively. Figure 8 shows the plot of φ_0/φ vs. silver concentration at constant DMDBMAD concentration. The value of the quenching constant is found as $K_{SV} = 99\times10^3\ M^{-1}$. The linearity of the Stern-Volmer plot indicates that only one type of quenching occurs in the system. There is no possibility of formation

of static quenching complexes via attractive electrostatic interaction between fluorophore-quencher pairs collisional (dynamic) quenching is effectively possible. In the presence of Ag NPs there is no change in the peak position in the absorption spectra of the DMDBMAD, the possibility of static quenching is absent. The absence a new broad band indicates that DMDBMAD has been bound to silver nanoparticles and so has failed to exhibit excimer and exciplex formation due to intermolecular interactions or if there is the formation of any trace of the excimer, it is also quenched by the metal. The Stern-Volmer quenching constant by silver nanoparticles in the solution is high indicating the presence of adsorption of the DMDBMAD molecule on the Ag surface. The high quenching efficiency of the solution results from the larger surface area provided by the smaller nanoparticles, which enhances their DMDBMAD adsorption capability.

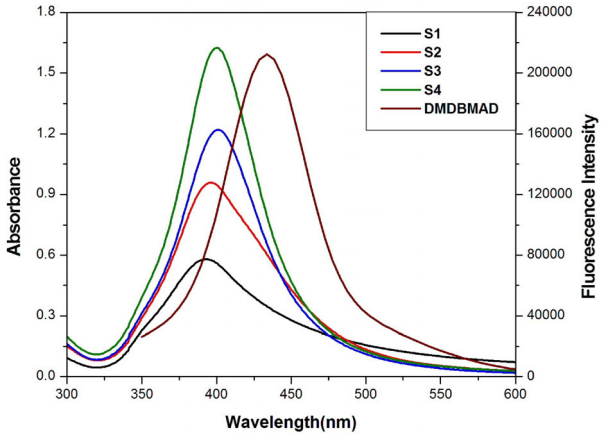

Fig. 9. Optical absorption spectra of Ag NPs and fluorescence emission spectrum of DMDBMAD in methanol.

3.7 FRET between acceptor and donor

Förster resonance energy transfer is a distance dependent interaction between the different electronic excited states of dye molecules in which excitation energy is transferred from one molecule (donor) to another molecule (acceptor) at the cost of emission from the former molecular system. According to Förster theory, the rate of energy transfer is based on the spectral overlap between emission spectrum of the fluorophore and absorption spectra of the Ag NPs, the relative orientation of the donor and acceptor transition dipoles, the distance between the donor and acceptor transition dipoles and the fluorescence quantum yield of the donor. It results in long range dipole-dipole interactions between the donor and acceptor [3,39].

In order to understand energy transfer, we have calculated the distance between NPs and DMDBMAD molecules using the Förster mechanism of non-radiative energy transfer. According to Förster theory, the energy transfer efficiency is related not only to the distance between the acceptor and donor but also to the Förster energy transfer distance, is given by:

$$E = 1 - \frac{F}{F_0} = \frac{R_0^6}{R_0^6 + r_0^6} \tag{1}$$

where F is the fluorescence intensity of the DMDBMAD in the presence of the acceptor, F_0 is the fluorescence intensity of the DMDBMAD in the absence of the acceptor. R_0 is the Förster radius or critical distance, is the characteristic distance at a FRET efficiency of 50%, which varies for different FRET pairs and r_0 is the distance between the acceptor and donor. FRET efficiency is close to maximum at distances less than R_0 and minimum for distances greater than R_0.

$$R_0^6 = 8.8 \times 10^{-25} k^2 n^{-4} \varphi \; J\,(\lambda) \tag{2}$$

where k^2 is the spatial orientation factor of the dipole, n is the refractive index of the medium, φ is the fluorescence quantum yield of the donor and J is the overlap integral of the fluorescence emission spectrum of the donor and absorption spectra of the acceptor was given by:

$$J\;(\lambda) = \frac{\int_0^\infty F\;(\lambda)\;\varepsilon\;(\lambda)\;\lambda^4 d\lambda}{\int_0^\infty F\;(\lambda)\;d\lambda} \tag{3}$$

where $F\,(\lambda)$ is the fluorescence intensity of the fluorescence donor at wavelength (λ) and $\varepsilon(\lambda)$ is the molar absorptivity of the acceptor at wavelength (λ).

The overlap of the optical absorption spectra of Ag NPs and the fluorescence emission spectrum of DMDBMAD were shown in Figure 9. The small spectral overlap between donor emission and acceptor absorption in the DMDBMAD/Ag NPs blends indicates that energy transfer is inefficient, and that a Förster-type energy transfer is unfeasible from the molecules of the DMDBMAD to the Ag NPs. Figure 9 also shows that acceptor weakly absorbed the excitation photon (330 nm), which may also contribute to the fluorescence intensity of Ag NPs. Despite the possibility of electron energy transfer, this mechanism, however is considered significant because of weak overlap between emission of donor and absorbance of acceptor. The calculated values of the energy transfer parameters are presented in Table 1. From the overlapping spectrum of the absorption spectra of acceptor and the fluorescence spectrum of DMDBMAD, $J\,(\lambda)$ can be evaluated by integrating the spectra from 350 to 600 nm. By adding the donor molecule into acceptor molecule, the fluorescence spectra shifts toward shorter wavelength providing a larger value of spectral overlap integral. The decrease in $J\,(\lambda)$ in turn causes a decrease in FRET efficiency. The value of $J\,(\lambda)$ changes from 2.11×10^{-14} cm^3 L mol^{-1} to 1.25×10^{-14} cm^3 L mol^{-1} with increase in the size of the Ag NPs from S1 to S4. Accordingly the energy transfer efficiency (E) between Ag NPs and DMDBMAD varies from 100% to 92%. It is evident that the efficiency of energy transfer is higher in S1 than that in S4. The critical distance between Ag NPs and DMDBMAD for S1 is 198 nm and 181 nm for S4, respectively. This high value

of R_0 is responsible for r_0 and energy efficiency values. The large values of R_0 indicate that the dominant mechanism responsible for energy transfer is long range dipole-dipole energy transfer (Förster-type) [40]. The distance between Ag NPs and DMDBMAD for S1 is 104 nm and 87 nm for S4, respectively. Interestingly it was observed that the FRET efficiency decreases with increasing $AgNO_3$ concentration. In present system FRET parameters mainly depend on size of the Ag NPs.

4 Conclusion

Silver NPs of different sizes from 9 nm to 17 nm were synthesized by Creighton method. The optical and morphological properties of the prepared nanoparticles were characterized by absorption spectroscopy and transmission microscopy. Fluorescence quenching of DMDBMAD molecule was analyzed by emission spectroscopy, it shows that the attachment of DMDBMAD molecules on the silver surface which leads to quenching of fluorescence. As the concentration of silver nitrate increases, it affects the fluorescence intensity of DMDBMAD. The quenching and association constants were calculated from Stern-Volmer and Benesi-Hildebrand plots. Ag NPs have dynamic quenching nature on the fluorescence of DMDBMAD. The distance between DMDBMAD to Ag NPs and the critical energy transfer distance were calculated using Förster theory and it depends on size of the Ag NPs. The study on interaction of DMDBMAD molecules with Ag NPs is a useful phenomenon and this system could open up the possible applications in integration of nanoscience with biology and medicine. Quenching property of the Ag NPs can be used for textile dyeing waste water treatments.

We gratefully acknowledge the financial assistance received from UGC-MRP and DST-CURIE, New Delhi, India for carrying out this research work.

References

1. J. Yang, A. Dass, A.M.M. Rawashdeh, C.S. Leventis, M.J. Panzner, D.S. Tyson, J.D. Kinder, N. Leventis, Chem. Mater. **16**, 3457 (2004)
2. S. Mallakpoor, A.R. Hajipoor, A.R. Mahdavian, S. Khoee, J. Appl. Polym. Sci. **76**, 240 (2000)
3. J.R. Lakowicz, *Principles of Fluorescence Spectroscopy*, 3rd edn. (Springer, New York, 2006)
4. J.W. Lown, Chem. Soc. Rev. **22**, 165 (1993)
5. J. Yguerabide, E. Yguerabide, Anal. Biochem. **262**, 137 (1998)
6. S. Eustis, M.A. El-Sayed, Chem. Soc. Rev. **35**, 209 (2006)
7. J.R. Lakowicz, B.P. Maliwal, J. Malicka, Z. Gryczynski, I. Gryczynski, J. Fluoresc. **314**, 431 (2002)
8. I. Brodie, C.A. Spindt, *Advances in Electronics and Electron Physics* (Academic Press, San Diego, 1992)
9. M. Umadevi, N.A. Sridevi, A.S. Sharmila, B.J.M. Rajkumar, M.B. Mary, P. Vanelle, O. Khoumeri, J. Fluoresc. **20**, 153 (2010)
10. M. Umadevi, P. Vanelle, T. Terme, B.J.M. Rajkumar, V. Ramakrishnan, J. Fluoresc. **19**, 3 (2009)
11. M. Umadevi, S.R. Kavitha, P. Vanelle, T. Terme, Plasmonics **8**, 859 (2013)
12. M. Umadevi, S.R. Kavitha, P. Vanelle, T. Terme, O. Khoumeri, J. Lumin. **142**, 1 (2013)
13. S.R. Kavitha, M. Umadevi, P. Vanelle, T. Terme, O. Khoumeri, Plasmonics **9**, 443 (2014)
14. S.R. Kavitha, M. Umadevi, P. Vanelle, T. Terme, O. Khoumeri, B. Sridhar, J. Spectrochim. Acta Part A **133**, 472 (2014)
15. J.A. Creighton, C.G. Blatchford, M.G. Albrecht, J. Chem. Soc. Faraday Trans. **75**, 790 (1979)
16. O. Khoumeri, M. Montana, T. Terme, P. Vanelle, Tetrahedron **64**, 11237 (2008)
17. P.B. Kandagal, S. Ashoka, J. Seetharamappa, S.M.T. Shaikh, Y. Jadegoud, O.B. Ijare, J. Pharm. Biomed. Anal. **41**, 393 (2006)
18. A.J. Haes, W.P. Hall, L. Chang, W.L. Klein, R.P. Van Duyne, Nano Lett. **4**, 1029 (2004)
19. G. Mie, Ann. Phys. **25**, 377 (1908)
20. D.S. Wang, M. Kerker, H. Chew, Appl. Opt. **19**, 2135 (1990)
21. S.L. Smitha, K.M. Nissamudeen, D. Philip, K.G. Gopchandran, J. Spectrochim. Acta Part A **71**, 186 (2008)
22. S. Yamamot, K. Fujiwara, H. Watari, J. Analyt. Sci. **20**, 1347 (2004)
23. J.J. Mock, M. Barbic, D.R. Smith, D.A. Schultz, S. Schultz, J. Chem. Phys. **116**, 6755 (2002)
24. A. Henglein, J. Phys. Chem. **97**, 5457 (1993)
25. A. Henglein, Chem. Mater. **10**, 444 (1998)
26. G. Aronuto, Appl. Organomet. Chem. **15**, 344 (2001)
27. G. Aronuto, G. Marletta, L. Nicolais, J. Mater. Sci. Lett. **20**, 663 (2001)
28. Z.L. Wang, J. Phys. Chem. B **104**, 1153 (2000)
29. S. Link, M.A. El-Sayed, Ann. Rev. Phys. Chem. **54**, 331 (2003)
30. H.A. Benesi, J.H. Hildebrand, J. Am. Chem. Soc. **71**, 2703 (1949)
31. S.K. Ghosh, A. Pal, S. Kundu, S. Nath, T. Pal, Chem. Phys. Lett. **395**, 366 (2004)
32. C.D. Geddes, H. Cao, I. Gryczynski, Z. Gryczynski, J. Fang, J.R. Lakowicz, J. Phys. Chem. A **107**, 3443 (2003)
33. J.R. Lakowicz, Anal. Biochem. **337**, 171 (2005)
34. H. Ditlbacher, J.R. Krenn, N. Felidj, B. Lamprecht, G. Schider, M. Salerno, A. Leitner, F.R. Aussenegg, Appl. Phys. Lett. **80**, 404 (2002)
35. J. Gersten, A. Nitzan, J. Chem. Phys. **75**, 1139 (1981)
36. Y. Chen, K. Munechika, D.S. Ginger, Nano Lett. **7**, 690 (2007)
37. R. Carminati, J.J. Greffet, C. Henkel, J.M. Vigoureux, Opt. Commun. **261**, 368 (2006)
38. D.A. Weitz, S. Garoff, J.I. Gersten, A. Nitzan, J. Chem. Phys. **78**, 5324 (1983)
39. T. Förster, *Modern Quantum Chemistry* (Academic Press, New York, 1965)
40. G.A. Kumar, V. Thomas, G. Jose, N.V. Unnikrishnan, V.P.N. Nampoori, J. Photochem. Photobiol. A: Chem. **153**, 145 (2002)